Astron. Nachr. / AN **333**, No. 9, 901 – 910 (2012) / **DOI** 10.1002/asna.201211727

Gregor@night: The future high-resolution stellar spectrograph for the GREGOR solar telescope

K.G. Strassmeier[1,⋆], **I.V. Ilyin**[1], **M. Woche**[1], **T. Granzer**[1], **M. Weber**[1], **J. Weingrill**[1], **S.-M. Bauer**[1], **E. Popow**[1], **C. Denker**[1], **W. Schmidt**[2], **O. von der Lühe**[2], **S. Berdyugina**[2], **M. Collados**[3], **P. Koubsky**[4], **T. Hackman**[5], and **M.J. Mantere**[6]

[1] Leibniz-Institut für Astrophysik Potsdam (AIP), An der Sternwarte 16, D-14482 Potsdam, Germany
[2] Kiepenheuer-Institut für Sonnenphysik (KIS), Schöneckstr. 6, D-79104 Freiburg, Germany
[3] Instituto de Astrofisica de Canarias (IAC), E-38200 La Laguna, Spain
[4] Astronomical Institute, Academy of Sciences, Fričova 298, CR-25165 Ondřejov, Czech Republic
[5] Finnish Centre for Astronomy with ESO (FINCA), University of Turku, Väisäläntie 20, FI-21500 Piikkiö, Finland
[6] University of Helsinki, Dept. of Physics, Gustaf Hällströminkatu 21, FI-00014 Helsinki, Finland

Received 2012 Aug 17, accepted 2012 Sep 23
Published online 2012 Nov 2

Key words instrumentation: spectrographs – stars: activity – stars: rotation – techniques: spectroscopic – telescopes

We describe the future night-time spectrograph for the GREGOR solar telescope and present its science core projects. The spectrograph provides a 3-pixel resolution of up to $R = 87\,000$ in 45 échelle orders covering the wavelength range 390–900 nm with three grating settings. An iodine cell can be used for high-precision radial velocity work in the 500–630 nm range. The operation of the spectrograph and the telescope will be fully automated without the presence of humans during night-time and will be based on the successful STELLA control system. Future upgrades include a second optical camera for even higher spectral resolution, a Stokes-V polarimeter and a link to the laser-frequency comb at the Vacuum Tower Telescope. The night-time core projects are a study of the angular-momentum evolution of "The Sun in Time" and a continuation of our long-term Doppler imaging of active stars.

1 Introduction

Recent "decadal reviews" for solar and stellar physics (e.g. Schrijver et al. 2009) emphasized the need for high spatial and spectral resolution observations in combination with three-dimensional (M)HD simulations for global physical parameters wider than just those for today's Sun. Stellar observations naturally focus on this global aspect and we add to GREGOR the technical capability to also observe other stars. Detailed comparisons of global solar parameters with those of other stars already revealed similarities but also differences not or not fully understood. The existence of spots near the rotational poles of other stars is one example. Another example is the angular-momentum loss of the Sun in time and the puzzle of the large dispersion of observed rotation periods in open clusters. Whether such a dispersion is just the product of the complex interplay between rotation and anisotropic turbulence, manifested as surface and radial differential rotation and meridional flows, or has additional physical agents like exoplanets remains to be determined. In any case, differential rotation alone is recognized as one of the key drivers for magnetic dynamo activity of the Sun and other stars (see, e.g., Rüdiger & Hollerbach 2009). It appears advisable to better quantify global and differential rotation also on other stars, in particular as a function of age.

The capability to indirectly resolve stellar surfaces and its spots by means of Doppler imaging became center stage for the quantitative exploration of the solar-stellar connection. Despite that starspots can not be observed with the same detail as sunspots, and consequently only the extremes of starspots are known (e.g. Strassmeier 2009), common physical mechanisms for their formation and evolution must apply. Observing selected stars with properties similar to the Sun, but at different ages and for long periods of time with sufficient time sampling, most likely will allow us to better understand the evolution of stellar angular momentum and its relation to the magnetic brake. Our long-term goal is to provide more quantitative observations of "The Sun in Time" (Guinan & Engle 2009) and thus to continue on the success of the National Solar Observatory McMath-Pierce night-time program in the late eighties (Smith 1986).

The aim of the present paper is to give an overview of the implementation of the night-time spectrograph. In Sect. 2, we lay out the general science case and describe the two main observational projects. In Sect. 3, a description of the spectrograph components is given. In Sect. 4, we summarize the upgrade plan and estimate the expected performance while in Sect. 5 the operations model is laid out. We summarize the current status again in Sect. 6.

⋆ Corresponding author: kstrassmeier@aip.de

2 Key science topics with Gregor@night

2.1 The Sun in time

Dorren, Güdel & Guinan (1995), and later Ribas et al. (2005), selected a handful of bright solar-type field stars on the basis of their coronal X-ray luminosity that resemble an approximate age sequence when converted to $L_{\rm X} \propto P_{\rm rot}^{-2}$, a relation found earlier by several other investigators. The current sample is 13 stars, including the Sun, and manifests an age sequence dubbed "The Sun in Time". There are a number of basic shortcomings with this sample, most notably their notoriously uncertain ages. For our present approach, we propose to overcome this by observing open-cluster stars of well-known age.

Among the first steps is a sample definition of cluster stars suitable for high-resolution spectroscopy with a 1.5-m telescope. This requires knowledge of the cluster age, the rotational period of the star, the $uvby\beta$ indices and, of course, radial velocities to verify the cluster membership and to exclude spectroscopic binaries. Most of these data are already being obtained within the STELLA/WiFSIP Open Cluster Survey (SOCS; see Fügner et al. 2011) currently carried out by one of our two robotic STELLA telescopes in the immediate neighborhood of GREGOR. We note that V-band magnitudes for a G2 star range between 8–16 mag for clusters of age and distance between that of the Hyades and the almost 2 Gyr of NGC 7789. The historical search for solar twins with high-resolution spectroscopy already included some open clusters, e.g., Barrett et al. (2001) presented a list of 14 "solar twins" in M 67 while Friel et al. (2003) studied four giants in Collinder 261.

Our aim is to obtain at least a few high-quality optical spectra of several hundred solar-type stars with known rotation period from the SOCS. The age range is thereby limited by the distance of the cluster but may extend to ≈2 Gyr. We aim for as many stars per cluster as possible in order to cover the 0.6–1.2 $M_\odot$ mass range but will be limited due to finite size of the telescope and the relatively long cadence needed for high-resolution, high signal-to-noise ratio spectra.

2.2 High-latitude magnetic activity on other stars

Given the strict low-latitude appearance of sunspots and their short lifetime of a month on average, it was a surprise to find long-lived big polar spots on other stars (Vogt & Penrod 1983; Strassmeier 1990). Such active regions may have lifetimes of over a decade in RS CVn binaries as well as in young main-sequence stars. Holzwarth, Mackay & Jardine (2006) suggested that polar spots are likely due to the influence of strong meridional circulation (polewards on the surface) and that the intermingling of polarities in the polar regions favors the higher flow velocities needed for that scenario. Obviously, polar spots could have a different formation history than low-to-mid latitude spots. Işik, Schmitt & Schüssler's (2007, 2011) coupled model of magnetic flux generation and transport verifies the increasing pole-ward deflection of emerging flux tubes with high angular velocities (e.g. Granzer et al. 2000) but also supports the polar magnetic-region accumulation picture put forward by Schrijver & Title (2001). Meridional transport of such flux would lead to strong polar fields. Whether these fields could be related to the discovery of high-latitude kG fields even on the Sun (Tsuneta et al. 2008) remains to be determined. While theory predicts that the meridional flow speed drops with faster rotation (Küker & Stix 2001), polar spots are particularly seen on rapidly rotating stars. This contradiction is yet to be explored, theoretically as well as observationally, but systematic observations will provide empirical limits.

Fig. 1 (online colour at: www.an-journal.org) The SoFINe spectrograph after dismounting from the Cassegrain focus of the NOT. The overall dimensions in meters are indicated. The instrument is shown on its trolly in zenith-pointing position with the circular telescope flange at the top. This spectrograph will be the base of the new Gregor@night instrument.

The great importance of long-term studies with high cadence is most evident in detecting and understanding stellar magnetic cycles. One major finding has been the fact that the strengths of spatially adjacent spot regions may flip forth and back as demonstrated e.g. for II Peg (Berdyugina et al. 1998, Hackman et al. 2012). The active longitudes on the same stellar hemisphere are predicted to be of opposite polarities (Tuominen et al. 2002; Elstner & Korhonen 2005), in agreement with observations. The dynamo solutions for such cases are not completely stationary in time. An azimuthal dynamo wave, causing the magnetic field either to speed up or lag behind in the rotational frame of the star, is seen in a majority of the models. Again, such a behavior has also been identified from Doppler maps (e.g. Lindborg et al. 2001). Furthermore, the analysis of II Peg suggested that a switch in the magnetic field polarity occurred when the activity level was low (Hackman et al. 2011). This could be a sign of an "active-star Hale polarity rule", as suggested by Tuominen et al. (2002), i.e. an analogue to the bipolar sunspot polarity rule but different in scale and being a global phenomenon. We do not know yet how these polarity switches are related to a possible stellar cycle.

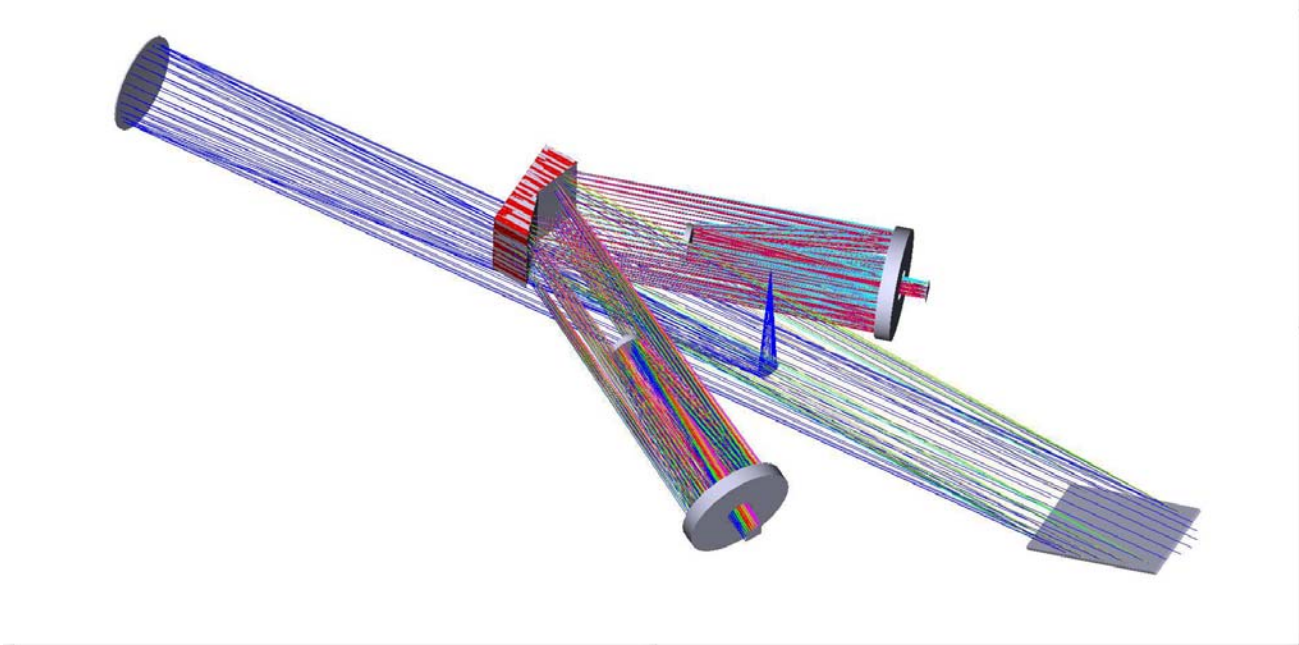

Fig. 2 (online colour at: www.an-journal.org) Zemax design of the refurbished SoFINe spectrograph, now called Gregor@night. The light injection is in the middle of the figure and from the "top" just before a 90-degree bent of the beam. The grating is to the right and the collimator to the left side of the picture. The cross disperser prism is seen in the middle in two positions feeding either one of two reflective cameras.

3 Current instrument status

3.1 General layout

The basis of Gregor@night is the high resolution échelle spectrograph SoFINe (Soviet-Finish spectrograph), originally in use at the Cassegrain focus of the Nordic Optical Telescope (NOT) at La Palma but decommissioned in fall 2012. It will be refurbished and upgraded at AIP in 2013 and then adapted for use with the GREGOR telescope in 2014. The spectrograph was designed and manufactured at the Crimean Astrophysical Observatory in collaboration with the Observatory of the Helsinki University and was installed at the Cassegrain focus of the 2.56 m NOT in June 1991 (Tuominen 1992). The spectrograph was designed to allow stellar spectroscopy with three different spectral resolutions R of 30 000, 80 000, and 170 000 for the NOT. The resolution is altered by exchanging optical cameras while all other optical elements of the spectrograph remain unchanged. Two of the three cameras are mounted permanently. This classical design had resulted in large light losses due to the comparable narrow slit widths, amounting to 65 % in the workhorse mode with the medium resolution camera #2. The spectrograph is equipped with a cross-dispersion prism in reflective double pass to separate spectral orders so that many different wavelengths are recorded in a single CCD exposure. The medium-resolution camera records 40 échelle orders with a length of 4.5 nm each. The change of the spectral setting is done by turning the echelle grating and the cross-dispersion prism. All components of the spectrograph are assembled in a rigid welded construction of dimension $1800\times800\times800$ mm (see Fig. 1); the total weight without the CCD dewars is 240 kg. The components of the spectrograph in its current configuration are described in detail by Ilyin (2000). In the following, we give a brief review of the major components.

3.2 The base spectrograph

Figure 2 shows the optical design. A diagonal folding mirror is located 300 mm behind the entrance slit and bends the optical axis by 98° into the entrance slit unit. The aluminum coated slit plane is tilted with respect to the optical axis by 13.5° in order to be viewed by the guiding camera. The slit width is remotely controlled while the width of the decker must be changed manually and defines the height of spectral orders and the inter-order spacing. The field-of-view of the guider is currently 70″. The shutter, grey filter, and open diaphragm are installed on a remotely controlled linear shaft. This filter and shutter unit consists of a hollow cylinder with two radial slots attached to the axis of a stepper motor and a turret wheel with eight holdings for filters. Filters have 16 mm in diameter and can be 6 mm thick. All of these filters are removed now. The beam switcher from target to Th-Ar or flat-field lamps consists of a pentaprism attached to the stepper motor axis via a rotating arm.

The optional circular polarimeter was described just recently by Ilyin (2012) and consists of a superachromatic, 400–680 nm, quarter-wave retarder of Pancharatnam design with five stretched PMMA acrylic films (Samoylov et al. 2004). The retarder is located on a rotary stage and turned by a stepper motor with a resolution of 15′. It follows by

the polarization beam splitter made of the calcite plate with its entrance surface cut at 45° with respect to its optic axis and was manufactured by B. Halle Nachfl. GmbH. The optic axis of the beam splitter is aligned with respect to the slit and the thickness of the calcite provides sufficient separation of two orthogonally polarized orders up to a wavelength of 700 nm.

The R2 échelle grating from Milton Roy Co., USA, has a grooved area of 128×256 mm and is ruled with 79 grooves per mm. Its blaze angle is $63.^\circ435$. The incident and diffracted beams are separated by a fixed angle of 8° and the angles are coplanar with the echelle normal. The échelle-tilt mechanism changes the angle of incidence by turning the frame around ball-edged pivots within $\pm3^\circ$ by driving the tangent arm attached to the axis of the remotely controlled stepping motor. The motor step size is about one pixel on the CCD for the long camera. The working spectral orders are 20–65 (1130–350 nm). The parabolic collimator mirror has a diameter of 128 mm and a focal length of 1396 mm.

The double-pass cross-dispersion prism is made of LF5 glass and mounted 800 mm apart from the echelle grating. The prism apex angle is 20.0° which makes order separations ranging from 60 pixels at 700 nm to 140 pixels at 380 nm. It allows 24 double-polarized orders to be recorded on the CCD. The positioning mechanism of the prism is similar to that of the echelle grating and allows changing the spectral setting in the cross-dispersion direction. The prism assembly is mounted on a mechanism which turns the prism around the optical axis to redirect the refracted beam to one of the two optical cameras installed simultaneously.

Three optical cameras provide three different spectral resolutions; two of them can be installed in the optical ports at the same time and the resolution is altered by flipping the cross-dispersion prism. The short (#3) and long cameras (#1) are inter changeable, whereas the medium camera (#2) is mounted permanently. The long optical camera is a Cassegrain mirror system with an effective focal length of 2079 mm and designed to provide a resolving power of $\approx$170 000. Slit width is $0.28''$ or 38 μm. It provides 15 échelle orders with a length of 2 nm at 500 nm. The medium optical camera is a Ritchey-Chrétien system with an effective focal length of 1000 mm for a spectral resolution of $\approx$80 000. Slit width in the NOT setup is $0.48''$ or 65 μm for 3-pixel sampling. It provides 40 échelle orders with a length of 4.5 nm at 500 nm. The short optical camera is a meniscus system (two menisci and two mirrors), has an effective focal length of 348 mm and provides a spectral resolution of $\approx$27 000. Slit width is $1.73''$ or 236 μm. It contains all 45 echelle orders with a length of 12 nm at 500 nm. Each of these cameras is equipped with a focusing mechanism which is a turnable threaded ring to offset the image formed on the CCD along the optical axis whilst the positions of the optical elements of the camera remain unchanged.

The calibration sources include a tungsten flat-field lamp and a Th-Ar hollow cathode lamp manufactured by Juniper & Co., UK. All electronics, computers etc. are mounted in an external rack. The rack will be located in the entrance room to the fourth-floor GRIS[1] room. The new data archive hardware (10 TB RAID array) will be mounted in the same rack.

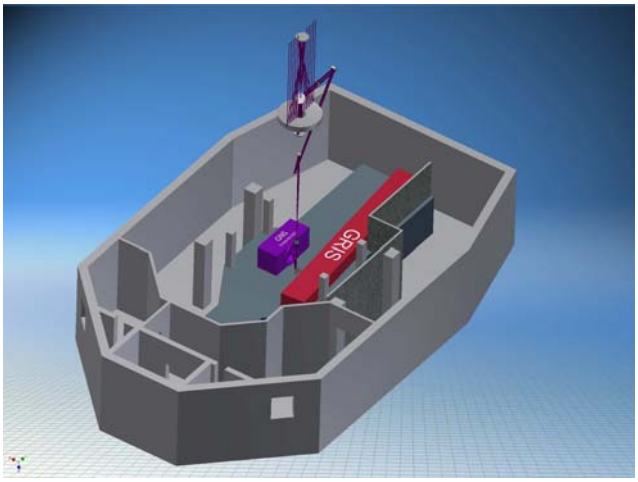

Fig. 3 (online colour at: www.an-journal.org) Physical location of Gregor@night. It is the smaller box with respect to the GRIS spectrograph whose optical table is shared. The telescope optical beam is shown in the night-time configuration, i.e. the F3 $f/41$ focus is occupied without the AO beam and without the image derotator but with the spectrograph fore optics. The total system until the spectrograph slit contains of 10 mirrors.

4 The upgrade: from SoFINe to even finer; Gregor@night

4.1 Overview

The upgrade will take up to three consecutive steps. The first step is done solely in the lab before delivery to GREGOR and includes the following action items:

1. Design and manufacture of a thermally and barometrically stabilized chamber for the spectrograph. It is to be located on the optical table of the building's fourth floor (see Fig. 3).
2. Mount the spectrograph and its welded enclosure in this chamber.
3. Add a focal-ratio transformation fore optics to convert the GREGOR f/41 beam to the spectrograph-collimator f/11 beam, including its mechanics.
4. Add a retractable iodine cell into the fore-optics assembly in order to reach the envisioned wavelength stability.
5. Replace the CCD for the permanently mounted camera #2 (focal length $f = 1$ m). This includes an e2v 2048×2048-pixel CCD and a new controller and dewar.
6. Install a closed-cycle CCD cooler and a vacuum pump for automated operation.

[1] GREGOR Infrared Spectropolarimeter; based on a horizontal Czerny-Turner spectrograph and the Tenerife Infrared Polarimeter TIP; see Collados et al. (2007), and also Collados et al. (2012).

7. Add new silver coatings to some of the reflective surfaces including a protection layer.
8. Add new anti-reflection coatings to critical transmission components.
9. Add a light pipe in front of the slit for scrambling issues.
10. Correct the originally out-of-the-field astigmatism of the original camera #2.
11. Replace the slit-viewing intensified TV camera with a proper CCD system.
12. Adapt the control electronics and interface to the night-time client.

The second step basically consists of a rigorous calibration plan to implement the regular use of the polarimeter for Stokes V. Details are to be determined. The third step includes the implementation of either camera #1 ($f = 2$ m) or camera #3 ($f = 0.35$ m) with a new CCD, a controller, and a dewar plus the setup of a high-precision, long-term, wavelength calibration unit. The vision is to implement a fiber link from the existing laser-frequency comb at the VTT tailored for the wavelength range of camera #1. Calibration light shall be injected into the spectrograph simultaneously with the target light via a fiber link.

4.2 A new 2k×2k CCD and dewar

The new device is a CCD of the e2v 42-40 series with an enhanced astro broad-band coating. It was part of the former STELLA/SES CCD system which was replaced by a 4k device in May 2012. It is of excellent cosmetics and has a QE peak of above 90 %, even at 400 nm. Its pixel size is 13.5 μm. The device is read through two amplifiers with a Gen-II Copenhagen controller and achieves an effective read-out noise of as low as 3.5 electrons. The dewar is homemade and was manufactured at AIP.

The telescope scaling factor sets the slit-width scale of the spectrograph to effectively $1'' = 75\,\mu$m, compared to 136 μm at the NOT. The spectrograph scaling factor from slit scale to CCD scale is 0.540 for camera #2 and the new CCD. This sets the configurations for Gregor@night as given in Table 1.

The only unknown at the moment is the distance of the spectrograph focal plane to the new CCD housing flange. A new mechanical flange must be manufactured that fits the dewar, the bayonet connectors on the spectrograph side, and the larger dimension of the dewar window. The dewar window itself must also be re-manufactured because the previous window had a wedge shape.

Table 1 Spectrograph characteristics with camera #2 and the new 13.5- μm-pixel CCD; ST = slit transmission.

Pixel Sampling	Superpixel (μm)	R ($\lambda/\Delta\lambda$)	Slit Width (μm)	Slit Width ($''$)	ST (%)
2	27	130 000	50	0.65	65
3	40.5	87 000	75	1.0	80
4	54	65 000	100	1.3	90

a)

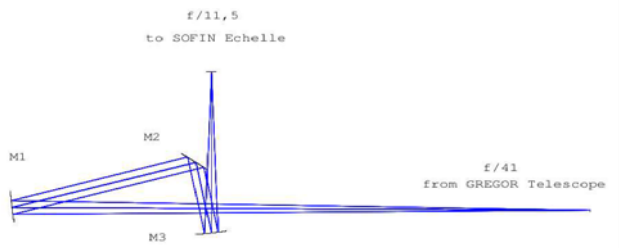

b)

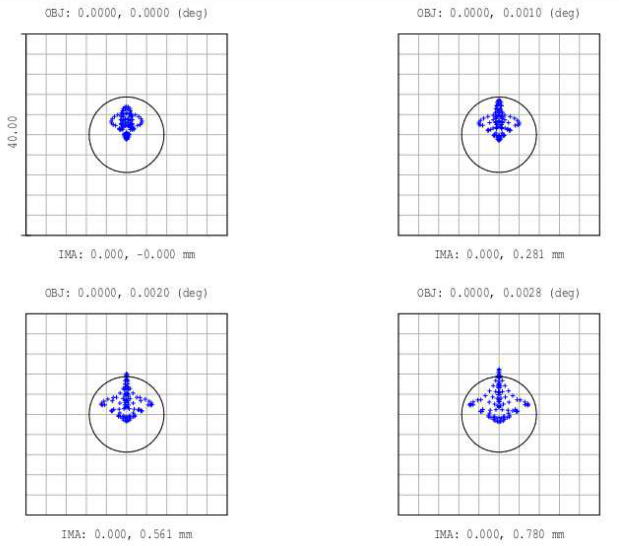

Fig. 4 (online colour at: www.an-journal.org) *a*) Design of the fore optics. It converts the $f/41$ telescope beam to the $f/11$ of the spectrograph collimator and consists of just three reflections. Two of the mirrors are off-axis parabola (M1 and M3) and one is a flat (M2). *b*) Spot diagram for the telescope plus the fore optics. Box size is 40 μm. Pluses are for the chief ray at 550 nm for four different field positions as indicated. The Airy disk radius (circle) is 7.5 μm.

4.3 Spectrograph fore optics

The telescope focal length is 58 950 mm and therefore the effective focal ratio is $f/40.94$ and the image scale becomes $3.50''$/mm. A cooled field stop at the prime focus (F1) reflects most of the sunlight upwards and transmits a field of view of $150''$ to the science focii. The night-time spectrograph is foreseen for the F3 coudé focus (Fig. 3). It is physically located in the fourth upper level of the building. It takes seven reflections and two AR-coated vacuum windows to reach the spectrograph fore-optics.

The spectrograph collimator has a f-ratio of $f/11$ and therefore the telescope focal ratio of $f/41$ must be transformed by a factor of ≈3.7 to match the spectrograph entrance. The new image scale is then 75 μm/$''$. Such a conversion could be achieved with a 5 – or more – lens refractive system for a comparable small field of view and a peak efficiency of only around 75 % (and maybe 65 % at 390 nm). Therefore, we decided on a fully reflective system for the

fore optics based on just three mirrors, with the disadvantage of being more expensive. A custom designed silver visual coating with UV enhancement on all three mirrors gives this sub system an average 91 % efficiency throughout the useful wavelength range of the spectrograph and still 88 % at 390 nm.

Figure 4a shows the detailed optical design of the fore optics, and Fig. 4b the expected spot diagram. Figure 5 shows the fore optics added to the telescope optics. The core of the optics is an off-axis parabola with an off-axis distance of 105 mm, a focal length of 400 mm and a free diameter of 65 mm. The two other components are a spherical mirror with a focal length of 2910 mm and a free diameter of 65 mm, and a circular plane mirror with $\lambda/10$ (peak-to-valley) at 633 nm and radius 64 mm. The system rms spots are 3.0 μm for the chief ray at 550 nm and 4.5 μm for the field edge at 780 nm.

4.4 Thermal housing

A passive thermal insulation cover encloses the entire spectrograph, the fore optics, and the iodine-cell assembly. The goal is to maintain a temperature within this "spectrograph chamber" that is constant to within $\pm 0.1^{\circ}$C over a day/night cycle. The insulation thickness is predetermined by the available space on the optical table. The optical table itself is located within the building on its own vibration-damped basement in a room that is already temperature controlled. To avoid a chimney effect at the light entrance hole into the "spectrograph chamber", the iodine cell will be used as a window during daytime but retracted during nighttime.

4.5 The iodine cell

The iodine cell will be inserted into the telescope beam between the F3 telescope focus and the first mirror of the fore-optics by means of a linear dish. Its usable spectral range is from 500 nm to 630 nm. Figure 6 shows the full spectral range of iodine absorption lines. The tube that holds the gas has a clear aperture of 40 mm and its length is 114 mm. Both entrance and exit surfaces are AR coated. Its production number is AS#3 of the ten cells that were produced for the Keck telescope (c/o S. Vogt, Lick Observatory). A reference spectrum at a resolution R of 1 million exists from NSO-McMath. The operation temperature is 50°C and requires an isolating cover. A copy of the APF system (the Lick Automated Planet Finder; Radovan et al. 2010) is produced for GREGOR.

4.6 The entrance slit unit

This unit serves several independent purposes. Firstly, it provides an image of the slit for the acquisition and guider camera. The current (intensified) TV camera is replaced by a Basler (acA1600-20) 1600×1200 mm, 4.4-μm CCD guiding camera. Secondly, an image scrambler will be attached

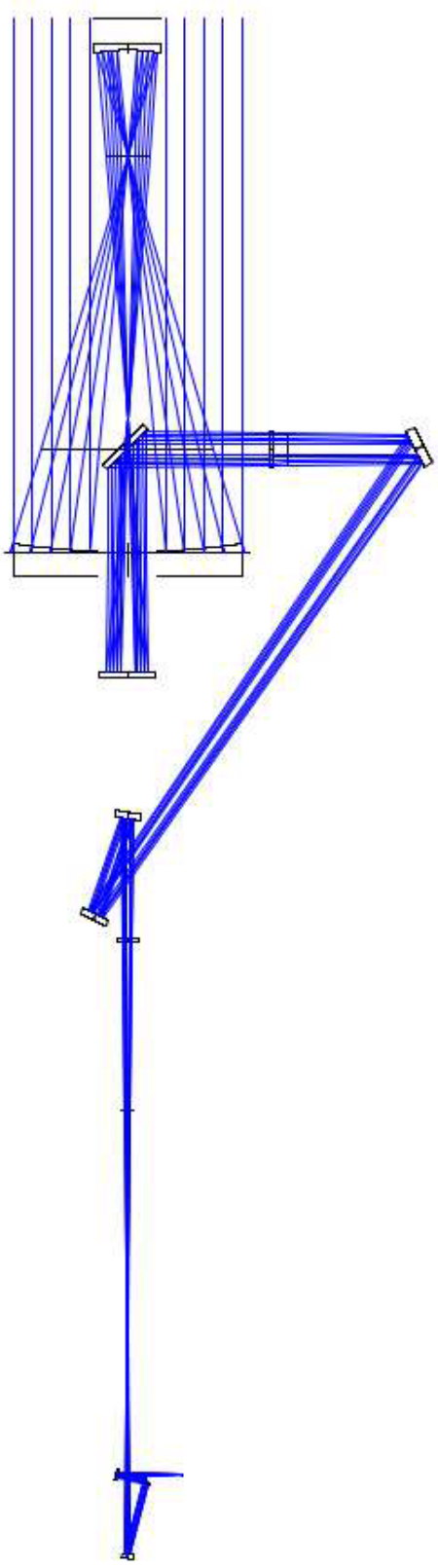

Fig. 5 (online colour at: www.an-journal.org) Zemax design of the full light path until the spectrograph entrance. The fore optics are the last three mirrors at the bottom, two of them off-axis parabola and one a flat (shown in detail in Fig. 4a).

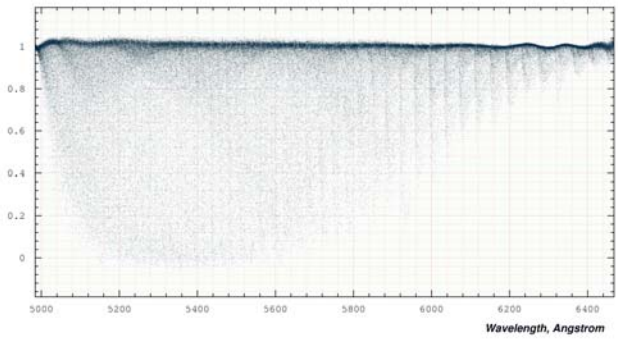

Fig. 6 (online colour at: www.an-journal.org) Full spectral range of the iodine-gas absorption for cell AS#3 in Gregor@night. The useful wavelength range with absorption lines is 500–630 nm.

to the slit jaws. It consists basically of a light pipe of length 50 mm.

4.7 Expected performance

Table 2 lists the expected transmission and reflection coefficients for all optical elements from the telescope's primary mirror (M1) to the spectrograph CCD. The iodine cell is optional and the cross disperser is in double pass with one reflection. A 13 % vignetting (87 % pseudo throughput) is due to overfilling of the échelle by the collimator. The folding mirror (FM) is outside the reflected beam from the collimator.

The values in Table 2 for M1–M4 are assumed from the CFHT washing experience and the tables in Magrath (1997). They assume that the protected-Al mirrors are washed once per year. The two entries dubbed "window" are the entrance and the exit windows of the telescope vacuum train. M5–M7 are within the vacuum train. Attempts are currently underway to silver coat the telescope mirrors except M1 and possibly also M2 which are in the open. In case M3–M7 have also UV-enhanced Ag coatings, then the telescope efficiency is raised to 57 % and the system efficiency telescope plus spectrograph increases from 9 % to 15 % at 600 nm.

Table 2 Telescope and spectrograph throughput. Abbreviations: Al = aluminum, Ag = silver, AR = antireflection, FM = folding mirror.

Optical Element	Material	Coating	Throughput (%)	
			390 nm	600 nm
M1	Zerodur	Al	89	87
M2	CeSiC	Al	89	87
M3	CeSiC	Al	89	87
M4	Zerodur	Al	89	87
Window	Suprasil	AR	98	98
M5	Zerodur	Al	90	89
M6	Zerodur	Al	90	89
M7	Zerodur	Al	90	89
Window	Suprasil	AR	98	98
M8	Zerodur	Ag	96	97
M9	Zerodur	Ag	96	97
M10	Zerodur	Ag	96	97
Telescope:			39	35
(I2 cell	glass	AR	90	90)
Slit	...	...	80	80
FM	Zerodur	Ag	92	97
Collimator	Zerodur	Ag	92	97
R2 grating	Zerodur		67	67
Vignetting			87	87
Cross disperser	LF5	Ag	73	73
Camera #2	Zerodur	Ag	85	94
Dewar window	Suprasil	AR	98	98
CCD			87	90
Spectrograph:			21	26
Total:			8	9

5 Operations

5.1 Nightly time line

All night-time observations are carried out in robotic mode, i.e. fully unattended. The switch from day-time operation to night-time operation requires four manual action items. Its time line is as follows:

1. Move the GREGOR image-derotator optics out of the beam.
2. Move the flat mirror of the AO-injection optics out of the beam.
3. Move any (day time) calibration-units out of the beam.
4. Switch to the night-time site control system SCS (includes dome control).

The next steps are already under control of the night-time client Site Control System (SCS; Granzer et al. 2001). It itself is a slave of two redundant weather stations, a dust sensor, and the STELLA all-sky infrared monitor (Weber et al. 2012b). For security reasons, it is foreseen that the mountain night-time crew is notified by SMS/e-mail in case the telescope/dome got stuck and immediate manual action is requested. In addition, the solar staff will be typically on site. Such dome closure or manual telescope movement with the hand panel overrides the SCS. We note that after six years of automated operation of the nearby STELLA building, such an override had not happened so far.

Among the first automated steps in the time line after the last manual step #4 is the (re)initialization of the telescope coordinate system and the determination of the telescope focus. This takes place late during twilight and will depend on the temperature of the telescope structure with respect to the night temperature and is an issue yet to be quantified. An initial calibration observation with a bright standard star will conclude the telescope set up. Master calibrations will be conducted during daytime (no telescope needed) and are

not part of the night time line. Infrequent pointing models are scheduled by the operator in Potsdam (see Granzer et al. 2012). At the end of the night the SCS moves the telescope to home position, closes the dome, and exits the interface to the telescope control system (Halbgewachs et al. 2012). All steps are logged and reported to the principal operator in Potsdam as well as to the GREGOR day-time crew on site. A GUI for manual override is active during night time operation.

5.2 Target scheduling

Scheduling follows the STELLA experience and also implements its software (see Granzer et al. 2001; Weber et al. 2012a). It uses a scheduling algorithm known as dispatch scheduling. From the entire pool of targets available, the algorithm calculates the actual merit for each target and then picks the object with the current highest merit. This per-target merit is a convolution of few initial priority classes and various time-dependent priorities. It weights the observational history, i.e. how many spectra already exist and how many more are needed to fulfill the task, the airmass, the anticipated slew time of the telescope, the remaining observing time in the current night or current season, bright versus dark time, the user balance, etc.. The only principal difference to the STELLA scheduling is the additional availability of an iodine cell and different grating positions for Gregor@night.

Once the scheduler has selected the target that should be observed next, a work-flow engine takes over and links the target-specific information into the appropriate sequencing template. Commands are then send timely to the subsystems, allowing for parallel or pure sequential execution of the specific tasks (see Granzer 2004). The observable targets and the work-flow templates reside as XML documents in a PSQL database and/or as files locally on the SCS.

5.3 Standard science observing mode

At least during the first year(s) of operation, only one standard science mode will be available. It is based on camera #2 and a slit width of 75 μm according to 1″ on the sky and a 3-pixel resolution of $R = 87\,000$. The optical camera and the size of the new CCD are still too small to cover the entire echelle format in both directions, in particular in the wavelength-dispersion direction. The cross-dispersion direction is fully covered (see Fig. 7). Therefore, we offer three wavelength settings according to three grating tilt angles to cover either the left half, the central part, or the right half of the echelle format. Default set-up will be the central part (centered on the blaze angle), dubbed grating position #1. The other set-up consists of two consecutive exposures, one in position #2 and one in position #3, which then can be combined to obtain almost full (optical) wavelength coverage. Note that Hα is observable only in setting #3.

All integrations in this mode come with wavelength gaps between the orders. These gaps increase with wavelength, as can be seen in Fig. 7. All central wavelengths fall on the blaze angle. For settings #2 and #3 the inter-order gaps start at approximately 600 nm and increase towards red wavelengths.

5.4 Iodine-cell science observing mode

The iodine-cell science mode is offered only for grating position #1. From the spectrograph side it is identical to the default science mode with grating position #1 (see above). The practical difference is that a spectrum in this mode is intended to obtain a precise radial velocity rather than a regular high-S/N spectrum. Therefore, its exposure time is typically much shorter than for the standard science mode because typical S/N ratios of ≈30:1 are sufficient for this purpose. The wavelength range of the iodine absorption at 50 °C is 500–630 nm (Fig. 6). This means that only orders #36 (central wavelength 627 nm) through #45 (central wavelength 502 nm) can be used for radial-velocity work.

5.5 Calibration modes

Standard calibration frames (halogen, Th-Ar arcs, and biases) will be taken during day time every day. During bad weather periods continuous Th-Ar frames and long-exposure dark frames will be taken during night-time. The reduction package will provide a global wavelength solution for every science frame. The standard flat-field frames taken during day time are used to construct a "running" master flat field that itself is then used for the data reduction. The total time coverage for a master flat is to be determined. Standard bias sequences are also taken throughout day time. Occasional dark frames with shutter closed are executed during day time. A user does not need to plan for any calibration frames unless for very specific purposes. Such specific calibration frames will be treated by the scheduler as targets and added to a user's time account.

The telescope will spent more on-sky time on calibration than a typical, manually operated telescope. Several standard stars will be scheduled nightly and are part of the quality-monitoring "engineering" modus. These targets include mostly radial-velocity standards, flux standards and bright B-type stars. Ironically, day-time spectra with the night-time spectrograph will not be possible due to the conflict with the solar, day-time operation of GREGOR.

5.6 Data reduction

The Advanced Acquisition, Archiving, and Analysis (4A) software package is also the main tool for providing observations with Gregor@night and its subsequent reduction and analysis of the data. The package provides the software to control the spectrograph and the CCDs which are used to register the echelle spectra. The software is described in detail in Ilyin (2000). It is foreseen that all raw data will be locally archived through the GREGOR data server, currently

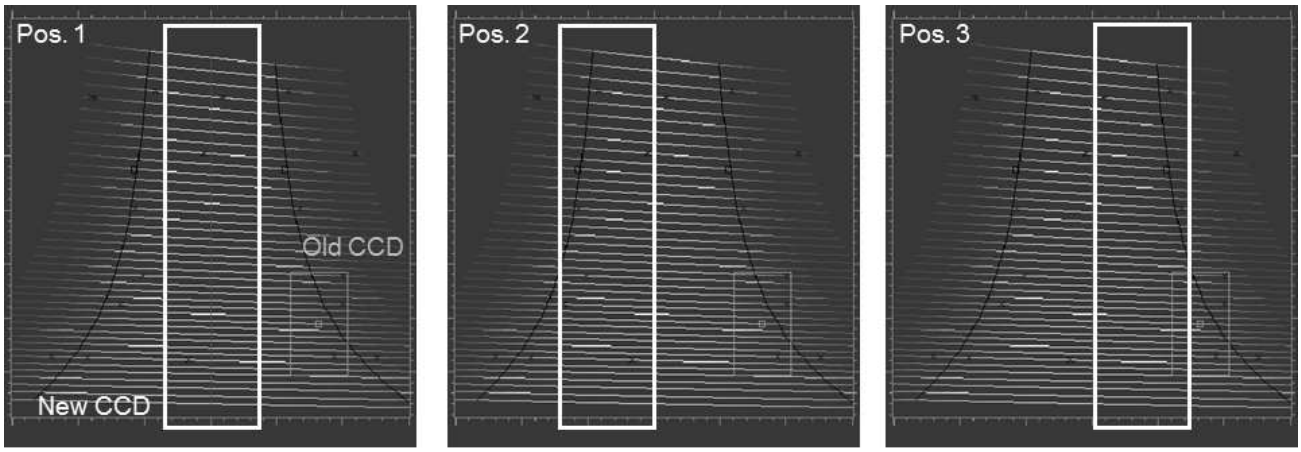

Fig. 7 Echelle coverage for three different grating tilts dubbed Position 1, 2, and 3 (*from left to right*). Shown is the size of the new e2v 2k×2k CCD with 13.5 μm pixels (large white box) compared to the old CCD (EEV 1200×330 pixels). Note that the scales for the two axes are not identical and thus the squared CCD appears as a an elongated box.

located at the neighboring VTT, as well as at the Media and Communications Center at AIP in Potsdam.

6 Summary

The SoFINe spectrograph of the 2.56 m NOT is being refurbished, upgraded, and recommissioned to become the Gregor@night spectrograph for the 1.5 m GREGOR solar telescope. Commissioning is foreseen for 2014. The instrument is a stellar spectrograph optimized for a spectral resolution of ≈87 000 with 3-pixel sampling and a 1″ slit width. It requires three exposures to cover most of the cross dispersion and the wavelengths of the echelle grating but principally ranges from 360–1130 nm. Due to its automated operation, only three fixed grating tilts will be offered for the 87 000 spectral resolution mode. More complexity is not foreseen for the first upgrade step despite that the spectrograph is principally capable of providing higher spectral resolutions of up to 170 000 for selected wavelength bins. The niche of our telescope-instrument combination is its long-term availability and consequently, we will use it for a dedicated study of "The Sun in Time", appropriate for a solar telescope. Other programs with focus on the solar-stellar connection will be executed on a time-share basis.

Acknowledgements. We thank the entire GREGOR consortium for their continuous and enjoyable collaboration. In particular, we thank our outgoing project manager Reiner Volkmer. We also appreciate the initiative of Carsten Denker that led to this issue of AN. The 1.5-meter solar telescope GREGOR was build by a German consortium under the leadership of the Kiepenheuer-Institut für Sonnenphysik in Freiburg with the Leibniz-Institut für Astrophysik Potsdam, the Institut für Astrophysik Göttingen, and the Max-Planck-Institut für Sonnensystemforschung in Katlenburg-Lindau as partners, and with contributions by the Instituto de Astrofísica de Canarias and the Astronomical Institute of the Academy of Sciences of the Czech Republic.

References

Barrett, E.A., Boesgaard, A.M., King, J.R., Deliyannis, C.P.: 2001, BAAS 199, 5710
Berdyugina, S.V., Berdyugin, A.V., Ilyin, I., Tuominen, I.: 1998, A&A 340, 437
Collados, M., Lagg, A., Díaz García, J.J., Hernández Suárez, E., López López, R., Páez Mañá, E., Solanki, S.K.: 2007, in: P. Heinzel, I. Dorotovic, R.J. Rutten (eds.), *The Physics of Chromospheric Plasmas*, ASPC 368, p. 611
Collados, M., López, R., Páez, E., et al.: 2012, AN 333, 872
Dorren, J.D., Güdel, M., Guinan, E.F.: 1995, ApJ 448, 432
Elstner, D., Korhonen, H.: 2005, AN 326, 278
Friel, E.D., Jacobson, H.R., Barrett, E., Fullton, L., Balachandran, S.C., Pilachowski, C.A.: 2003, AJ 126, 2372
Fügner, D., Granzer, T., Strassmeier, K.G.: 2011, in: C.M. Johns-Krull, M.K. Browning, A.A. West (eds.), *Cool Stars, Stellar Systems, and the Sun*, ASPC 448, p. 863
Granzer, T., Caligari, P., Schüssler, M., Strassmeier, K.G.: 2000, A&A 355, 1087
Granzer, T., Weber, M., Strassmeier, K.G.: 2001, AN 322, 295
Granzer, T.: 2004, AN 325, 513
Granzer, T., Halbgewachs, C., Volkmer, R., Soltau, D.: 2012, AN 333, 823
Guinan, E.F., Engle, S.G.: 2009, in: E.E. Mamajek, D. Soderblom (eds.), *The Ages of Stars*, IAU Symp. 258, p. 395
Hackman, T., Mantere, M.J., Jetsu, L., et al.: 2011, AN 332, 859
Hackman, T., Mantere, M.J., Lindborg, M., Ilyin, I., Kochukhov, O., Piskunov, N., Tuominen, I.: 2012, A&A 538, A126
Halbgewachs, C., Caligari, P., Glogowski, K., et al.: 2012, AN 333, 840
Holzwarth, V., Mackay, D.H., Jardine, M.: 2006, MNRAS 369, 1703
Ilyin, I.V.: 2000, PhD Thesis, Univ. Oulu, Finland; see http://www.aip.de/People/ilyin/sofin/sofin/sofin.html
Ilyin, I.V.: 2012, AN 333, 213
Işik, E., Schmitt, D., Schüssler, M.: 2007, AN 328, 1111
Işik, E., Schmitt, D., Schüssler, M.: 2011, A&A 528, A135
Küker, M., Stix, M.: 2001, A&A 366, 668
Lindborg, M., Korpi, M.J., Hackman, T., et al.: 2011, A&A 526, A44
Magrath, B.: 1997, PASP 109, 303

Radovan, M.V., Cabak, G.F., Laiterman, L.H., Lockwood, C.T., Vogt, S.S.: 2010, in: I.S. McLean, S.K. Ramsay, H. Takami (eds.), *Ground-based and Airborne Instrumentation for Astronomy III*, SPIE 7735, p. 77354K
Ribas, I., Guinan, E.F., Güdel, M., Audard, M.: 2005, ApJ 622, 680
Rüdiger, G., Hollerbach, R.: 2004, *The Magnetic Universe*, Wiley VCH, Weinheim
Samoylov, A.V., Samoylov, V.S, Vidmachenko, A.P., Perekhod, A.V.: 2004, Journal of Quantitative Spectroscopy & Radiative Transfer 88, 319
Schrijver, C.J., Title, A.M.: 2001, ApJ 551, 1099
Schrijver, K., Carpenter, K., Karovska, M., et al.: 2009, *Astro2010: The Astronomy and Astrophysics Decadal Survey*, Science White Papers, no. 262
Smith, M.A.: 1986, in: M.S. Giampapa (ed.), *Prospects for a New Synoptic High Resolution Spectroscopic Observing Facility*, p. 124
Strassmeier, K.G.: 1990, ApJ 348, 682
Strassmeier, K.G.: 2009, A&AR 17, 251
Tsuneta, S., Ichimoto, K., Katsukawa, Y., et al.: 2008, ApJ 688, 1374
Tuominen, I.: 1992, NOT News 5, 15
Tuominen, I., Berdyugina, S.V., Korpi, M.J.: 2002, AN 323, 367
Vogt, S.S., Penrod, G.D.: 1983, PASP 95, 565
Weber, M., Granzer, T., Strassmeier, K.G.: 2012a, in: N.M. Radziwill, G. Chiozzi (eds.), *Software and Cyberinfrastructure for Astronomy II*, SPIE 8451, p. 84510K
Weber, M., Klebe, D., Strassmeier, K.G., Granzer, T., Blatherwick, R.D.: 2012b, in: *Observatory Operations: Strategies, Processes, and Systems IV*, SPIE 8448, p. 84481H

